NASA Technical Memorandum 110218

An Evaluation of the Measurement Requirements for an In-Situ Wake Vortex Detection System

Henri D. Fuhrmann and Eric C. Stewart
Langley Research Center, Hampton, Virginia

May 1996

National Aeronautics and
Space Administration
Langley Research Center
Hampton, Virginia 23681-0001

AN EVALUATION OF THE MEASUREMENT REQUIREMENTS FOR AN IN-SITU WAKE VORTEX DETECTION SYSTEM

Henri D. Fuhrmann
Eric C. Stewart
NASA Langley Research Center
Hampton, Virginia 23681-0001

Abstract

Results of a numerical simulation are presented to determine the feasibility of estimating the location and strength of a wake vortex from imperfect in-situ measurements. These estimates could be used to provide information to a pilot on how to avoid a hazardous wake vortex encounter. An iterative algorithm based on the method of secants was used to solve the four simultaneous equations describing the two-dimensional flow field around a pair of parallel counter-rotating vortices of equal and constant strength. The flow field information used by the algorithm could be derived from measurements from flow angle sensors mounted on the wing-tips of the detecting aircraft and an inertial navigation system. The study determined the propagated errors in the estimated location and strength of the vortex which resulted from random errors added to theoretically perfect measurements. The results are summarized in a series of charts and a table which make it possible to estimate these propagated errors for many practical situations. The situations include several generator-detector airplane combinations, different distances between the vortex and the detector airplane, as well as different levels of total measurement error.

Nomenclature

b_{det}	span of the detecting aircraft, ft.
b_{gen}	span of the generating aircraft, ft.
b_{sep}	separation distance between the vortex pair, ft.
C	numerical method cost function (see Eqn. 7), deg.
M	Measurement magnitude of flow field values (see eqn. 8), deg.
r	radius from the center of a vortex to the point of calculation (eqn. 3A), ft.
R	radius from the center of a vortex dipole to the point of calculation, ft.
V_{gen}	velocity of the generating aircraft, ft./sec.
V_{det}	velocity of the detecting aircraft, ft./sec.
v_θ	tangential velocity component at radius (r) of a vortex, ft./sec.
v	horizontal velocity component of the vortex flow field (eqn. 4), ft./sec. or deg.
v_{ideal}	theoretical horizontal velocity component of vortex flow field, ft./sec.
W_{gen}	weight of the generating aircraft, lb.
w	vertical velocity component of the vortex flow field (eqn. 3), deg.
w_{ideal}	theoretical vertical velocity component of vortex flow field, ft./sec.
y	horizontal position of the detecting aircraft, ft.
z	vertical position of the detecting aircraft, ft.
α	angle of attack at one wing tip due to one vortex, radians
β	angle of sideslip on one wing tip due to one vortex, radians
$\Delta\alpha$	differential angle of attack across span of detector airplane due to vortex, deg.
$\Delta\beta$	differential sideslip angle across span of detector airplane due to vortex, deg.
$\varepsilon_{\Delta\alpha}$	Error for $\Delta\alpha$ flow field value, deg.
$\varepsilon_{\Delta\beta}$	Error for $\Delta\beta$ flow field value, deg.
ε_w	Error for (w) flow field value, deg.
ε_v	Error for (v) flow field value, deg.
ε_{total}	Total flow field error (see eqn. 5), deg.
Γ	circulation strength of the vortex, $ft.^2/sec.$
ϕ	roll angle of the detecting aircraft, deg.
ρ	air density, $slug/ft^3$.)
θ	angle from the center of a vortex to a point of calculation, deg.
Subscripts	
i=1, 2, or 3	indicating the right wing tip, left wing tip, and centerline respectively.

j=1 or 2	indicating the right and left vortex respectively.
ideal	theoretical value with no measurement error
c	calculated value based on estimated vortex parameters

Abbreviations:

FAA	Federal Aviation Administration
IFR	Instrument Flight Rule
IMC	Instrument Meteorological Conditions
max	maximum value

Introduction

Recent studies have highlighted the costly airline delays at major airports due to limited airport capacity and air traffic congestion.[1] One factor contributing to these delays is the longitudinal spacing requirement between aircraft on approach to landing imposed by the Federal Aviation Administration (FAA) in Instrument Meteorological Conditions (IMC). These spacing requirements were defined so as to reduce the likelihood of hazardous wake vortex encounters by aircraft during takeoff and on approach to landing. Recognizing these separation requirements as a source of air traffic delays, the FAA has prompted a reevaluation of these standards. If the separation distances can safely be reduced a reduction in airport congestion and delays would ensue. A reduction in separation requirements is estimated to have a potential billion dollar a year savings for the nation's airlines.[2] Reduction of the spacing requirements, however, must be approached cautiously as several recent airplane incidents have been attributed to wake vortex disturbances.[3]

In the past, much effort was devoted to reducing the vortex hazard by modifying geometry or procedures of the airplane generating the vortex so as to attenuate the vortex to a level deemed safe[4]. However, none of these modifications have yet been shown to be practical[5]. More recently NASA has been studying means to increase airport capacity by predicting or sensing weather conditions when it will be safe to reduce the spacing requirements. An Aircraft Vortex Spacing System (AVOSS) has been proposed which will use measurements of weather conditions to predict when vortices will have decayed to a safe level or blown out of the approach corridor[6]. Although the AVOSS system will use ground-based measurements, air-borne measurements could also be useful. Airborne detection schemes may take the form of a modified windshear detection system using Doppler RADAR[7], or aerosol motion and velocity determination via Light Detection and Ranging (LIDAR). An alternate system using flow angle sensors and an inertial navigation system has been suggested. This study evaluates the concept of such a system to see if it could be sensitive enough to provide the pilot with information to allow evasive maneuvers to be executed.

Exploratory test flights have demonstrated the possibility of detecting wake vortices at substantial lateral distances with simple, low-cost wing tip flow monitoring devices.[8] Though no attempt to locate the vortex pair or to determine the vortex strength was performed in this study, the results show that adequate detection and maneuver time may be available.

Further analysis by Stewart[9] of this joint FAA/NASA flight test has revealed that flow angles alone are not sufficient for a unique determination of detecting aircraft location with respect to a vortex pair as had been previously theorized[10]. Additional information derived from inertial velocity measurements is also needed. With these measurements vortex velocities and velocity gradients can be determined.

Assuming the correct model of the vortex flow field is known, the strength and location of a wake vortex can be determined using exact measurements of the velocities and velocity gradients in the flow field. However, if the model is not correct or if the measurements are not perfect, the estimated location and strength of the wake vortex will be in error. The primary purpose of this paper is to determine how errors in the measurements propagate into errors in the estimated strength and location values determined for the wake vortex. With this information, the allowable measurement error can be determined for such a system to be feasible. The measurement error is a combination of instrumentation noise, atmospheric turbulence, and contamination due to aircraft motion.

The question of the correctness of the mathematical model of the wake vortex will not be addressed herein. For this paper, simulated data with known amounts of error will be used to evaluate the error propagation relationships using an iterative algorithm developed

for this study. The axes of the airplane are assumed to be aligned with the axes of the wake vortex allowing for the two-dimensional problem to be studied here. The algorithm is described and typical convergence rates are presented for different trajectories and measurement errors. The results are summarized in a series of charts and a table which make it possible to estimate these propagated errors for many practical situations. The situations include several generator-detector airplane combinations, different distances between the vortex and the detector airplane, as well as different levels of total measurement error.

Theory

A typical near-parallel approach to a vortex is studied in this paper and illustrated in figure 1. The aircraft generating the wake is denoted the generator aircraft, and the aircraft approaching the vortex pair is denoted the detector aircraft. A near-parallel vortex encounter is of primary concern because of the extreme roll angles and loss of altitude that can occur as a result of the rotational velocities in the vortex flow field. In some weather conditions a large airplane can generate a wake which can be dangerous for a long period of time[11]. The pilot of an aircraft entering a hazardous vortex encounter usually has no warning of the imminent danger. What may seem logical control inputs by the pilot or autopilot to counteract the effects of the vortex flow may actually exacerbate the problem as the aircraft traverses the flow field.

Flow Field Equations

In this study, the flow field created by the vortex dipole is modeled using potential theory. The flow field equations are explicitly derived by Stewart in reference 12 and are briefly presented in Appendix A. The vortex flow field geometry and terminology are presented in figure 2. This figure depicts a rear view of the parallel vortex encounter of concern, showing angular and radial position definitions.

Appendix A shows that from potential theory, the ideal vortex flow field parameters of differential angle of attack ($\Delta\alpha$), differential sideslip angle ($\Delta\beta$), vertical inertial velocity component (w), and horizontal inertial velocity (v) can be determined from the vortex parameters of location (y,z), vortex strength (Γ), and vortex pair separation distance (b_{sep}). Conversely, the vortex parameters defined as (Γ, y, z, b_{sep}) can be determined if the flow parameters ($\Delta\alpha$, $\Delta\beta$, w, v) are known. However, no closed form solution is known and an iterative scheme must be used.

Vortex Flow Field Characteristics

Solving iteratively for the solution to the flow field equations is a fairly straight-forward procedure. In order to gain more insight into solution convergence problems and vortex flow phenomena a more complete analysis of the flow field is necessary. The generator and detector aircraft characteristics to be used for the initial flow field analysis are the P3-PA28 combination presented in the fourth row of table 1. These are the characteristics for the aircraft used in the flight test of reference 8. Table 1 also presents span, weight, and vortex strengths for various aircraft combinations which will be discussed later.

The four flow field parameters are able to define the unique location of a given detecting aircraft with respect to a vortex pair. A representative cross-sectional vortex flow field map showing only the differential flow angle measurements ($\Delta\alpha$, $\Delta\beta$) is presented in figure 3. This map separates the flow field into 12 sectors defined by the values of the differential flow angle measurements ($\Delta\alpha$, $\Delta\beta$). The lines separating each sector are locus of points at which one of the differential flow angle values is zero. As was concluded in reference 9, a unique radial location of a detecting aircraft unfortunately cannot be determined from $\Delta\alpha$ and $\Delta\beta$ alone. Any one of three possible radial locations can have the same differential flow angle measurements. However, adding vertical and horizontal vortex velocity components (w,v) yields a flow field map separated into 16 sectors based on the signs of the measured flow field values as shown in figure 4. Each sector represents a unique combination of signs of the flow field parameters and each location defines unique combinations of the flow field parameter values. Again, the lines denoting sector separations are the locus of points at which one or two of the four flow field parameter values is zero.

Examination of these flow field maps reveals a way to reduce the number of iterations required of the wake vortex detection algorithm to converge on a solution. The positive and negative sign combinations of the four flow field values can be used to quickly resolve the

angular location of a detecting aircraft with respect to the vortex pair. This sector location method was used to provide initial estimates of the solution parameters (y, z). However, the existence of a vortex was not considered to be established until a converged solution was obtained using the iterative algorithm.

Wake Vortex Location Algorithm

The wake vortex detection and location algorithm is composed of (1) an initialization routine, (2) vortex flow field equations module, and (3) an iterative scheme for converging on the estimate of the vortex parameters. This algorithm is explained in more detail in appendix B.

The code was compiled and run on various systems. The results of this study are from a SUN IPX with a fixed computational power of 28.5 MIPS or 4.2 MFLOPS.

Error Evaluation Procedure

This section describes the procedure used to evaluate the effects of measurement error on the accuracy of the vortex parameter solution. The detecting airplane was assumed to be traveling in the same general direction as the axis of the wake vortex but with small velocities in the plane perpendicular to the axis. The span (b_{det}), velocity (V_{det}), and roll attitude (ϕ) of the detecting aircraft are taken to be known quantities. For simplicity in this study, the roll angle of the detecting aircraft is fixed at zero.

The first step was to calculate a series of ideal flow field values ($\Delta\alpha_{ideal}$, $\Delta\beta_{ideal}$, w_{ideal}, v_{ideal}) along a given trajectory with an assumed set of vortex parameters. This assumed set of vortex parameters was retained for comparison with estimated vortex parameters.

The second step was to add random errors to the ideal flow field parameters as shown in the following equations.

$$\Delta\alpha = \Delta\alpha_{ideal} + \varepsilon_{\Delta\alpha} \tag{1}$$

$$\Delta\beta = \Delta\beta_{ideal} + \varepsilon_{\Delta\beta} \tag{2}$$

Table 1: Aircraft pairs and characteristics (V_{gen}=V_{det}=200 ft./sec.)

Aircraft Pairs (Generator-Detector)	b_{gen}-b_{det} ft.	W_{gen}-W_{det} lb.	Γ_{gen} $ft^2./sec.$
737-737	94.8 - 94.8	114,000 - 114,000	3840
MD11-MD80	169.5 - 108	430,000 - 128,000	8075
747-737	211 - 94.8	574,000 - 114,000	8659
P3-PA28	100.3 - 34.5	95,500 - 2,200	2494
757-Citation	124.8 - 53.5	198,000 - 20,000	5050
757-737	124.8 - 94.8	198,000 - 114,000	5050
757-C182	124.8 - 40	198,000 - 3,500	5050
757-Corporate Jet	124.8 - 43.8	198,000 - 18,000	5050
757(heavy)-Corporate jet	124.8 - 43.8	217,348 - 18,000	5543
MD11(mod)-MD80	169.5 - 108	395,044 - 128,000	7418

$$w = \left(\frac{w_{ideal}}{V_{det}} x57.3 + \varepsilon_w \right) \quad (3)$$

$$v = \left(\frac{v_{ideal}}{V_{det}} x57.3 + \varepsilon_v \right) \quad (4)$$

Where $\varepsilon_{\Delta\alpha}$, $\varepsilon_{\Delta\beta}$, ε_w, and ε_v were random errors uniformly distributed about zero. The total error (ε_{total}) in degrees was defined as,

$$\varepsilon_{total} = \sqrt{((\varepsilon_{\Delta\alpha_{max}})^2 + (\varepsilon_{\Delta\beta_{max}})^2 + (\varepsilon_{w_{max}})^2 + (\varepsilon_{v_{max}})^2)} \quad (5)$$

where the maximum values of the distribution of each flow field error were assumed to be equal such that,

$$\left| \frac{\varepsilon_{total}}{2} \right| = \left| (\varepsilon_{\Delta\dot{\alpha}_{max}}) \right| = \left| (\varepsilon_{\Delta\beta_{max}}) \right| = \left| (\varepsilon_{w_{max}}) \right| = \left| (\varepsilon_{v_{max}}) \right| \quad (6)$$

The next step was to determine the vortex parameters for these perturbed flow field parameters using the iterative routine. The iteration scheme attempts to minimize a cost function of the form,

$$C = \sqrt{(\Delta\alpha - \Delta\alpha_c)^2 + (\Delta\beta - \Delta\beta_c)^2 + (w - w_c)^2 + (v - v_c)^2} \quad (7)$$

where subscript (c) denotes a calculated value based on estimated vortex parameters

The final step was to statistically summarize these vortex parameters for a given radius from the vortex dipole center.

Vortex Approach Characteristics

In the following cases the vortex approach simulation was based on the P3-PA28 combination of detecting and generating aircraft as presented in the fourth row of table 1.

Linear Aircraft Position Solutions

The first set of position solutions presented in figure 5 are those along the line from the first quadrant to the second quadrant at 20, 100, and 200 feet above the vortex pair. Solutions were attempted every 4 feet along each trajectory. The total error, ε_{total} remained constant at 0.02°. Figures 6 and 7 show similar linear position solutions along lines running vertically and diagonally through the flow field and vortex core.

The accuracy of the solutions are degraded at large distances, as well as in very near proximity to the centers of the vortices. For these test cases the solution positions match the actual trajectory well, and although solution quality is degraded at large distances, solutions exist even at 300 feet from the vortex dipole center.

Circular Aircraft Position Solutions

Figures 8 through 10 show circular aircraft solution positions for a constant radius of 200 feet from the center of the vortex dipole in the y-z plane. Solutions were obtained every 4 feet of arc length or 0.02 radians. The solution locations given by the algorithm are superimposed on the actual position track.

Figure 8 shows the solution locations superimposed on the actual positions for ε_{total}=0°. This test case demonstrates that the code works properly for input data with no error. Figure 9 presents a similar circular profile for an ε_{total}=0.01°. Converged solutions were obtained for 66% of the test points and correlation between the calculated and actual positions is very good. An interesting anomaly develops when the trajectory crosses the (y) or (z) axis where few and inaccurate solutions are obtained. This anomaly is examined in more detail later. Fig 10 may represent the limit of the detection capability for this specific condition (ε_{total}= 0.1°). Converged solutions were obtained for only 9% of the test points, but the solutions which were obtained do correlate with the circular track in general.

Figure 11 presents three circular position tracks at radii of 100, 200 and 300 feet at a constant total error ε_{total} = 0.01°. The solution accuracy, as expected, is reduced with increasing radius although even at a radius of 300 feet from the vortex center, some accurate solutions are

obtained. Areas of few solutions again appear along the y and z axes.

This effect is made more apparent in figure 12 showing the circular position track at a radius of 200 ft. and a measurement error of ε_{total}=0.05°. The y-axis is crossed at 180° and 360°, and the z-axis is crossed both at 90° and 270°. At these intersections we see considerable divergence from the actual position tracks. This may be due to the fact that along these axes, two of the four flow field parameters approach zero.

If a consistent set of previously converged solutions exist, trajectory prediction methods could possibly be employed to eliminate some erroneous solutions in these zones. However, an approach solely along one of these axes would result in fairly inaccurate solutions.

Generalization of Results

In order to generalize the results, a data base was compiled using the various aircraft pairs shown in table 1. The detecting aircraft was "flown" at a constant radius around the vortex pair and points were sampled every 4 feet. The radial distance of the detecting aircraft from the center of the vortex pair was parametrically increased from a radius of nearly one span to several spans of the detector aircraft. The convergence rate and solution accuracies were then recorded for each data point. The results for each constant radius position track were averaged and recorded for that radius. The results were then plotted against the average measurement magnitude (*M*) of the flow field values for each radius case and airplane combination. The measurement magnitude *M* is the square root of the sum of the squares of each of the ideal flow field values averaged over all aircraft positions at a constant radius.

$$M = \frac{\{ \sum_{i=1}^{N} (\sqrt{\Delta\alpha(i)^2_{ideal} + \Delta\beta(i)^2_{ideal} + w(i)^2_{ideal} + v(i)^2_{ideal}}) \}}{N} \tag{8}$$

where N = number of points in a given trajectory

The measurement magnitude was found to be a good parameter by which to correlate and generalize the convergence trends because it is a function of the vortex parameters (y, z, Γ, b_{sep}), which are determined by the generator airplane, and b_{det} which is determined by the detector airplane. The solution criteria appeared to be correlated with *M* and thus provides a generic way to estimate the convergence trends for specific aircraft combinations. Table 2 shows *M* values for various aircraft pair and radii.

Figure 13 presents the convergence rate trends with *M* for increasing total measurement error ε_{total}. The curves are fared through numerous data points which had significant scatter. The approximate level of scatter is indicated by the "Mean Error Displacement" on the figure. Using these trends, and the information in table 2, a quick estimate of the convergence rate and solution accuracy of a specific vortex approach may be ascertained.

Figure 14 presents similar correlations of location error versus *M*. Location error is defined as an average of the percent location error in the (y) and (z) directions. Although the location errors may be relatively large, all that is required is an approximate location of the vortex with respect to the aircraft for the information to be useful.

The values of average vortex strength error are presented in figure 15 for the same ε_{total} range. This parameter remains relatively constant between 40 and 100% for most of the range of measurement magnitude. Therefore, the measure of relative hazard the vortex may pose can be ascertained with a fair degree of confidence from the vortex strength solution. However, figure 16 shows that for the specific case of ε_{total}=0.33, average vortex pair separation error does not correlate well with *M*. This is true in the general case and may be a result of the convergence criteria set in the algorithm. However, with relative position and strength determined, vortex separation accuracy may not be as important.

Example applications

Two examples are now presented which demonstrate how this information might be used.

Example 1: Take what might be a potentially dangerous vortex encounter: that of a corporate jet on approach

behind a 757. Using table 2, or the vortex flow field equations, the average measurement magnitude *(M)* for these aircraft can be easily calculated for a given distance from the vortex pair. Now figure 13 can be employed to determine the minimum measurement error required to meet a certain early detection radius, and figure 14 used to ascertain the resulting location error.

Let us assume in this case that we want to give the pilot 7 seconds from first notification to avoid a direct encounter with the vortex core. If the lateral approach velocity is 20 ft./sec. or less, a minimum early detection radius of about 180 ft is necessary assuming the model breaks down at a radius of 40 ft. However a convergence rate of less than 100% increases the minimum early detection radius. If we assume a convergence rate of 20% and a sampling rate of 5 points/sec., the result will be a delay, on average, of about a second for the algorithm to converge on the vortex solution. We assume also that multiple solutions (3) are required before, an alert may be confidently sent to the pilot. This delay causes the delay to increase by 3 seconds which in turn makes the detection radius increase by another 60 feet to 240 feet. Table 2 gives us the *M* value of about 1.4° from which the required measurement accuracy can be determined from figure 13 (see example 1). In this case the intersection of 20% and 1.4 yields a measurement error which must fall below 0.8°. This does not fall outside the realm of current measurement capabilities as presented in reference 13. From figure 14 (example 1) we see that for *M*=1.4° and measurement error of 0.8° an average position solution error of about 90% will

Table 2: Values of average measurement magnitude *M* for various aircraft pair and radii

Aircraft Pairs (Generator-Detector)		Trajectory Radius (ft.) and *M* (degrees)									
737-737	R	81	114	148	181	215	248	282	315	348	382
	M	8.17	3.98	2.24	1.45	1.02	0.76	0.58	0.47	0.38	0.31
MD11-MD80	R	145	206	267	327	388	449	509	570	630	691
	M	6.78	3.15	1.84	1.21	0.86	0.64	0.49	0.39	0.32	0.27
747-737	R	181	257	333	408	484	560	636	711	787	863
	M	5.14	2.46	1.45	0.96	0.68	0.51	0.39	0.31	0.26	0.21
P3-PA28	R	86	121	157	192	228	263	299	334	370	405
	M	4.4	2.17	1.29	0.85	0.61	0.45	0.35	0.28	0.23	0.19
757-Citation	R	106	151	196	240	284	329	373	418	462	506
	M	7.33	3.53	2.09	1.38	0.98	0.73	0.57	0.45	0.37	0.31
757-737	R	107	151	196	240	284	329	373	417	462	506
	M	7.84	3.70	2.14	1.41	0.99	0.74	0.57	0.47	0.37	0.31
757-C182	R	107	151	196	240	284	329	373	417	462	506
	M	7.84	3.50	2.08	1.38	0.98	0.73	0.57	0.45	0.37	0.31
757-Corporate Jet	R	107	151	196	240	284	329	373	417	462	506
	M	7.21	3.51	2.08	1.38	0.98	0.73	0.57	0.45	0.37	0.31
757(heavy)-Corporate Jet	R	107	151	196	240	284	329	373	417	462	506
	M	7.92	3.85	2.28	1.51	1.07	0.80	0.62	0.50	0.41	0.34
MD11(mod)-MD80	R	145	206	267	327	388	449	509	570	630	691
	M	5.75	2.65	1.55	1.01	0.72	0.54	0.42	0.33	0.27	0.22

result. In summary, given the convergence rate required for early detection and avoidance, a measurement requirement and resulting solution error can be determined.

Example 2: Conversely, the avoidance time which can be provided the pilot can be estimated from the measurement error and allowable convergence rate. If one can measure the vortex flow with an accuracy of 0.33° (ε_{total}=0.33) and tolerate a 50% error in the solution location, then they can detect a vortex with a measurement magnitude *(M)* of 1.6° (fig. 14 example 2). This would have a convergence rate of approximately 35% (fig. 13). If one assumes a 747-737 combination of aircraft, this would correspond to a detection range of about 322 ft. (table 2). Assuming a closure rate of 20 feet per second, this would allow a pilot about 16 seconds to react from first alarm.

False Solutions

The probability that turbulence will cause the algorithm to converge on a false solution should be small. In other words, the algorithm should not ordinarily converge for measured values that do not have the unique signature of a vortex flow field. In this way the code would act as a filter against false alarms.

Algorithm testing on random turbulent flow field measurements showed that the code produces a false solution on turbulent values only 0.2% of the time. That is, the algorithm will "accidently" converge on a solution for a vortex flow field when given random turbulence measurement on average two out of every 1000 sampled points. This rate is probably acceptable if several consistent and consecutive solutions are required before an alarm is issued.

Concluding Remarks

A numerical simulation has been made to study the feasibility of using in-situ measurements to determine the location and strength of a wake vortex. Simulated measurements with different levels of noise or error were used to estimate the vortex location and strength using an iterative algorithm. The algorithm is intended for a pilot alarm which should be effective for slow encounter rates such as those which occur in near-parallel vortex encounters on landing approach. The specific conclusions of the present study are as follows:

1) The algorithm can provide reasonable estimates of vortex location and strength using simulated measurements with moderate amounts of error.

2) The quality of the estimates of the vortex characteristics and location decrease with increasing measurement error and distance from the vortex. The quality of the estimates was also poor in near proximity to the vortex pair.

3) The convergence rate of the algorithm decreased with increasing distance and error.

4) There are regions of the vortex field in which the vortex estimates are degraded independent of distance form the vortex.

5) The algorithm produces very few false solutions in simulated random turbulence and thus provides an effective filter against false alarms.

6) Tables and graphs are presented for several contemporary airplanes which provide a rapid means to estimate requirements for measurement error to achieve a specified convergence rate and solution accuracy.

7) The concept appears to provide the possibility of detecting, locating, and estimating the strength of a vortex at a distance which could provide a pilot with ample time to make an evasive maneuver for near-parallel encounters.

References

1. Page, Richard: *The Wake Vortex Problem Revisited.* In proceedings for Radio Technical Commission for Aeronautics Annual Assembly and Technical Symposium, December 1989.

2. Baart, Douglas; Monk, Helen; and Schweiker, Mary: *Airport Capacity and Delay Analyses.* U.S. Department of Transportation / Federal Aviation Administration, DOT / FAA / CT-TN91 / 18, April 1991.

3. Warwick, Graham: "FAA Questions 757 Vortex Separation." Flight International, January 18, 1994.

4. Rossow, Vernon J.: *Prospects for Alleviation of Hazard Posed by Lift-Generated Wakes.* Proceedings of Aircraft

Wake Vortices Conference, DOT/FAA/SD-92/1.1 or DOT-VNTSC-FAA-92-7.1, Washington, D.C. October 29-31, 1991.

5. Dunham, R. E., Jr.: *Unsuccessful Concepts for Aircraft Wake Vortex Minimization.* Wake Vortex Minimization, NASA SP-409, 1977, pp. 221-249.

6. Hinton, *D. A.: Aircraft Vortex Spacing System (AVOSS) Conceptual Design*. NASA TM 110184, August 1995.

7. Nespor, J. D., Hudson, B., Stegall, R. L., and Freedman, J. E.: *Doppler Radar Detection of Vortex Hazard Indicators.* Proceedings of Aircraft Wake Vortices Conference, DOT/FAA/SD-92/1.1 or DOT-VNTSC-FAA-92-7.1, Washington, D.C. October 29-31, 1991.

8. Branstetter, J. R.; Hastings, E. C.; and Patterson, J. C. Jr.: *Flight Test to Determine Feasibility of a Proposed Airborne Wake Vortex Detection Concept.* DOT/FAA/CT-TN 90/25, NASA TM 102672, April 1991.

9. Stewart, Eric C.: *A Comparison of Airborne Wake Vortex Detection Measurements with Values Predicted from Simple Theory*. NASA TP 3125, November 1991.

10. Bilanin, Alan J.; Milton, Teske E.; and Curtiss, Howard C. Jr.: *Feasibility of an Onboard Wake Vortex Avoidance System.* NASA CR 187521, April 1987.

11. Olsen, Goldburg, and Rogers, Aircraft Wake Turbulence, and its Detection, 1990.

12. Stewart, Eric C.: *Flight-Test Evaluation of a Direct-Measurement Airborne Wake-Vortex Detection Concept.* Proceedings of Aircraft Wake Vortices Conference, DOT/FAA/SD-92/1.1 or DOT-VNTSC-FAA-92-7.1, Washington, D.C. October 29-31, 1991.

13. Scott, M. A.; Strain, N. A.; Lee, C. C.: *Flight Evaluation of a Stagnation Detection Hot-Film Sensor.* AIAA Paper 92-4085, August, 1992.

14. Burden, Richard L.; and Faires, J. Douglas: *Numerical Analysis.* PWS Publishing Company, Boston, 1993.

Appendix A: Flow Field Equations

The assumptions used in the testing of the detection algorithm are: (1) the vortices remain parallel to each other and the ground plane, (2) strength is constant with time (no decay), (3) the vortex strength (Γ) and separation (b_{sep}) are given by eqns. 1A and 2A respectively which are derived assuming an elliptical lift distribution, (4) the effect of the detecting aircraft on the vortex flow field is assumed to be negligible, and (5) the longitudinal axis of the detecting aircraft is assumed to be parallel to the vortex pair.

The 2-dimensional vortex flow field geometry and terminology used herein are presented in figure 2. This figure depicts a rear view of the parallel vortex encounter of concern, showing angular and radial position definitions.

$$\Gamma = \frac{4}{\pi}\left(\frac{W_{gen}}{\rho \times V_{gen} \times b_{gen}}\right) \tag{1A}$$

$$b_{sep} = \frac{\pi}{4} \times b_{gen} \tag{2A}$$

$$v_{\theta_{i,j}} = \frac{\Gamma}{2\pi r_{i,j}} \tag{3A}$$

The tangential velocity component (equation 3A) of the jth vortex is resolved into vertical and horizontal velocities at the location of the ith wing-tip of the detecting aircraft. These velocity components are then used to calculate the vortex induced angle of attack $\alpha_{i,j}$ and angle of sideslip $\beta_{i,j}$ using a small angle approximation.

$$\alpha_{i,j} = \{\frac{v_{\theta_{i,j}}}{V_{det}}\}\ \{\cos\theta_{i,j}\cos\phi - \sin\theta_{i,j}\sin\phi\} \tag{4A}$$

$$\beta_{i,j} = \{\frac{v_{\theta_{i,j}}}{V_{det}}\}\ \{\sin\theta_{i,j}\cos\phi + \cos\theta_{i,j}\sin\phi\} \tag{5A}$$

Where the subscript (i) being either the number 1 or 2 representing the right or left wing tip respectively, and (j) is the number 1 or 2 referring to the right or left vortex.

Using equations (4A) and (5A) the difference in the angle of attack between the right and left wingtips ($\Delta\alpha_{ideal}$) and difference in the angle of sideslip ($\Delta\beta_{ideal}$) can be ascertained.

$$\Delta\alpha_{ideal} = [\,(\alpha_{\theta_{1,1}} + \alpha_{\theta_{1,2}}) - (\alpha_{\theta_{2,1}} + \alpha_{\theta_{2,2}})\,] \quad (6A)$$

$$\Delta\beta_{ideal} = [\,(\beta_{\theta_{1,1}} + \beta_{\theta_{1,2}}) - (\beta_{\theta_{2,1}} + \beta_{\theta_{2,2}})\,] \quad (7A)$$

Likewise, the velocity components at the center of the wing are given by

$$w_{ideal} = -(v_{\theta_{3,1}}\cos\theta_{3,1} + v_{\theta_{3,2}}\cos\theta_{3,2}) \quad (8A)$$

$$v_{ideal} = (v_{\theta_{3,1}}\sin\theta_{3,1} + v_{\theta_{3,2}}\sin\theta_{3,2}) \quad (9A)$$

where the subscript 3 corresponds to the center of the wing.

The resulting equations (6A-9A) represent the ideal vortex flow field parameters of differential angle of attack ($\Delta\alpha_{ideal}$), differential sideslip angle ($\Delta\beta_{ideal}$), vertical inertial velocity component (w_{ideal}), and horizontal inertial velocity (v_{ideal}). The question to be answered is, given measure values of these 4 flow parameters, whether location (y,z), vortex strength (Γ), and vortex pair separation distance (b_{sep}) can be adequately estimated using the subject algorithm.

The wake vortex detection and location algorithm works by solving these coupled, nonlinear simultaneous flow field equations (6 through 9) for the vortex state parameters (Γ, y, z, b_{sep}) using the measured flow field parameters ($\Delta\alpha$, $\Delta\beta$, w, v) given the span (b_{det}), velocity (V_{det}), and roll attitude (ϕ) of the detecting aircraft.

Appendix B: Wake Vortex Detection and Location Algorithm

The wake vortex detection and location algorithm is composed of (1) an initialization routine, (2) vortex flow field equations module (appendix A), and (3) an iterative scheme for converging on the solution.

State Parameter Initialization Routine

To help ensure convergence with the fewest number of iterations, an initialization routine is employed in the detection code. This routine generates initial values for the vortex state parameters (Γ, y, z, b_{sep}) using one of two methods. The first method (Start-Up Method) initializes the vortex state parameters using only information obtained from the flow field measurement devices whereas the second method (In-Process Method) utilizes previously converged solutions or an average of these solutions for a more precise estimate. The second method is more effective in reducing convergence time although the start-up method must be used if no previously converged solutions have been identified.

Start-Up Initialization Method

The first initialization method is based on the formulation derived by Bilanin, Teske, and Curtiss[10] which solves fairly accurately for two possible solution angles from the center of the vortex dipole but does not solve accurately for the radius.

$$y = \frac{2w}{\Delta\alpha\left(\frac{V_{det}}{b_{det}}\right)} \frac{(-1 + 3(f)^2)}{(1 - (f)^4)} \quad (1B)$$

$$z = f \times y \quad (2B)$$

$$f = \frac{w}{v}\left\{1 \pm \sqrt{1 + \left(\frac{v}{w}\right)^2}\right\} \quad (3B)$$

These equations (1B-3B) are used only to generate an initial aircraft location with respect to the vortex center (y,z) for the optimization routine. The vortex strength and separation distance between the vortices (Γ, b_{sep}) are initialized to constants based on average values for current transport aircraft. This method has been found to be sufficient for seeding the optimization routine.

In-Process Initialization Method

The second initialization routine for the optimization code is used when previously converged solutions are available. The previously converged values of the state parameters (Γ, y, z, b_{sep}) are used as the initial estimate

for subsequent iterations. This method becomes operative only after an initial convergence on a solution has been obtained.

Solver Routine

This routine is a general purpose routine to solve a set of non-linear simultaneous equations. It uses an iterative procedure based on the method of Secants and is used to solve for the vortex state parameters given the measured flow field values. The routine utilizes the same vortex flow field model as that used to generate the simulated measurement data. It minimizes the sum of the squares of the difference between the measured values of the flow field parameter and the flow field parameters calculated from the estimated vortex state parameters (equation 7). It estimates better values of the state parameters at each iteration by a 4-dimensional intercept and slope calculated using a secant approximation (reference 14).

When the values of the state parameters are such that the cost function of equation 7 is within a specified tolerance, the algorithm converges. If the algorithm becomes caught in a local minimum, or if a set maximum number of iterations is exceeded, then the algorithm does not converge on a solution. No other solver routines were used, however, other numerical method schemes may prove more efficient and effective than the nonlinear method of Secants scheme. These methods were not examined in this paper.

Figure 1. Parallel approach wake vortex encounter with typical velocity distributions from generator aircraft.

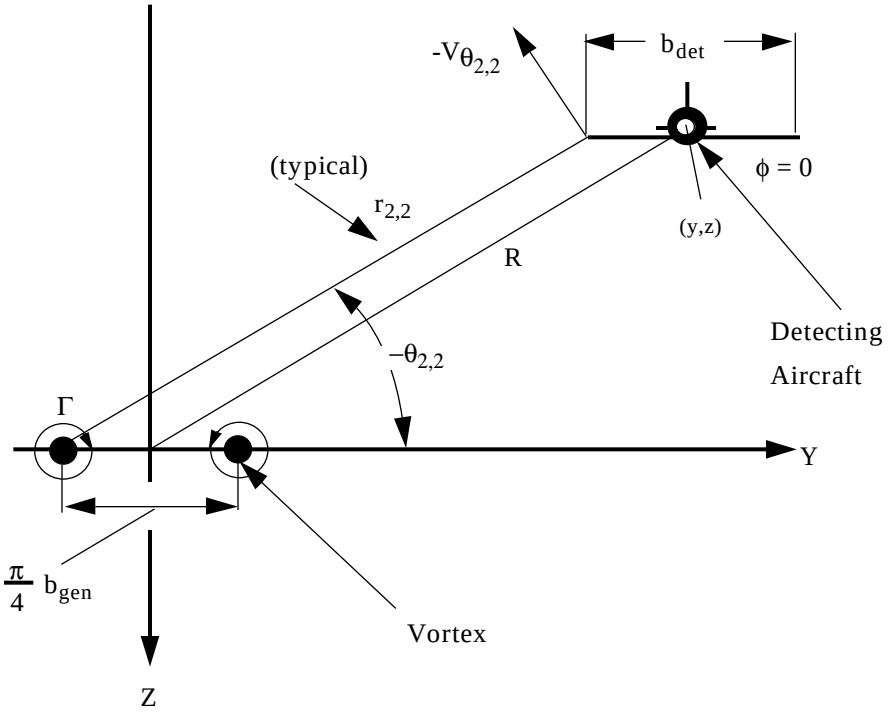

Figure 2. Aft view of wake vortex encounter showing terminology used in the analysis.

Figure 3. Twelve flow field sectors defined by the values of $\Delta\alpha$ and $\Delta\beta$. (P3-PA28)

Figure 4. Sixteen flow field sectors defined by the values of $\Delta\alpha$, $\Delta\beta$, w, and v. (P3-PA28)

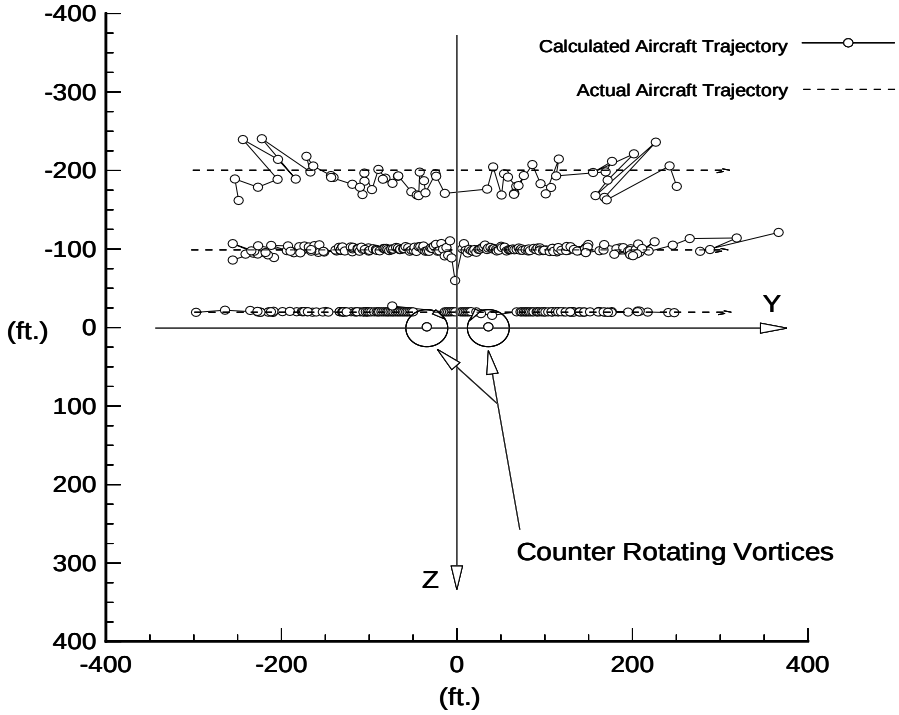

Figure 5. Horizontal vortex encounter position solutions with ε_{total}= 0.02°. (P3-PA28)

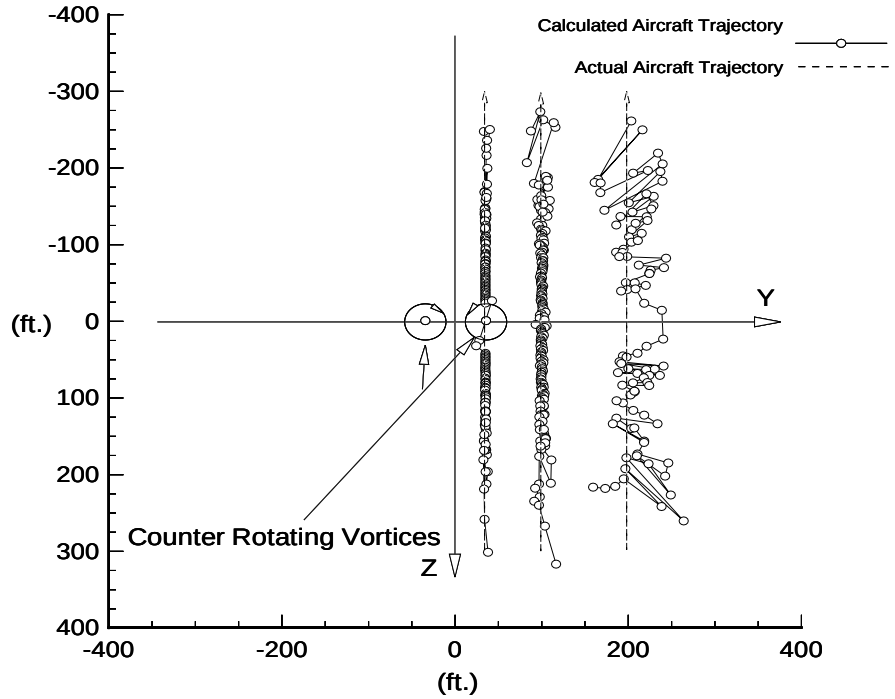

Figure 6. Vertical vortex encounter position solutions with ε_{total}= 0.02°. (P3-PA28)

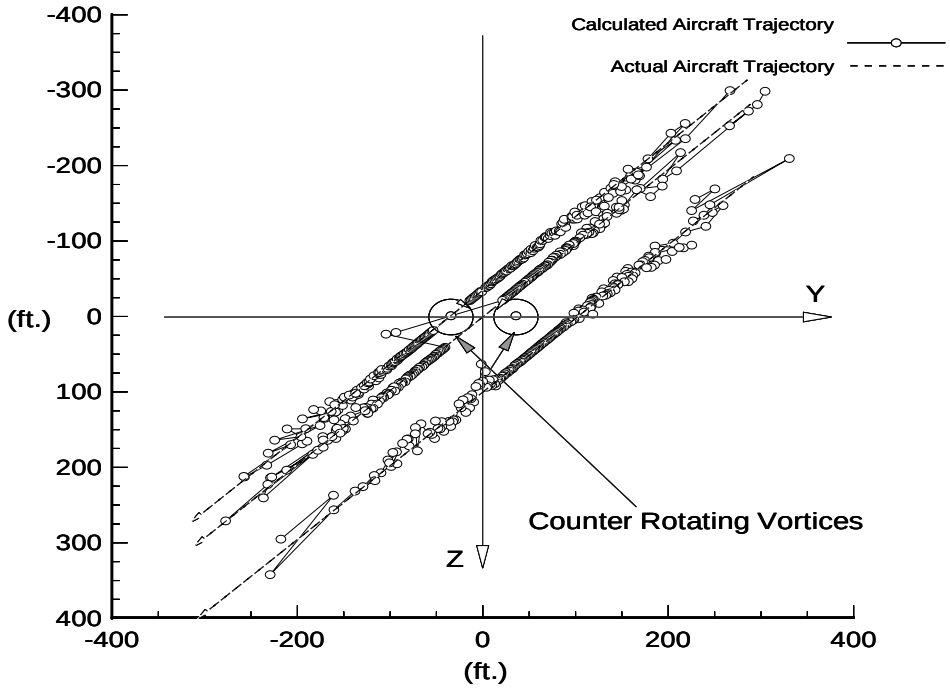

Figure 7. Diagonal vortex encounter position solutions with ε_{total}= 0.02°. (P3-PA28)

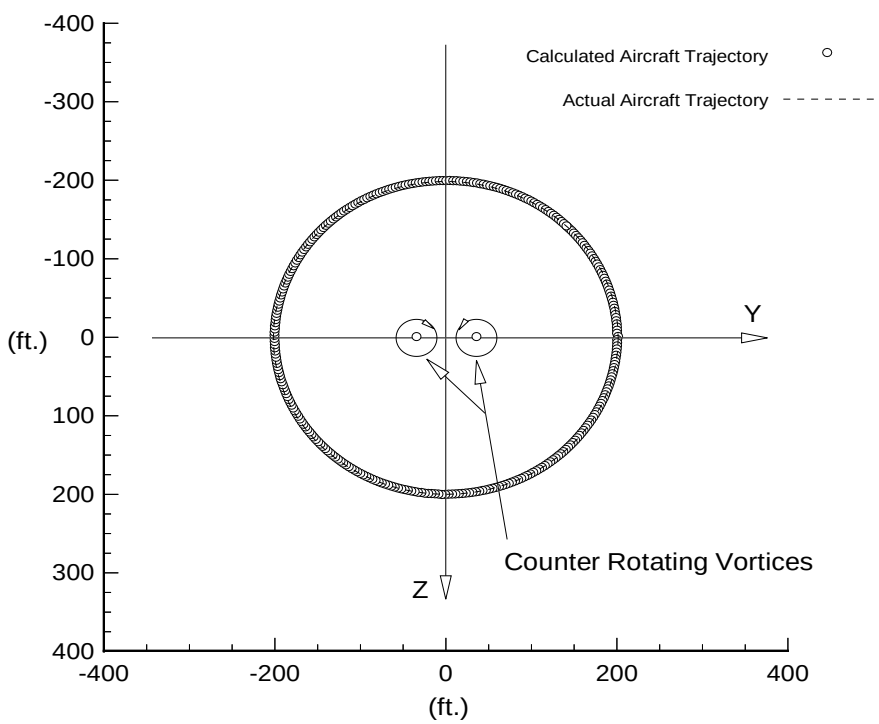

Figure 8. Circular wake vortex encounter track and position solutions with ε_{total}= 0.0°. (P3-PA28)

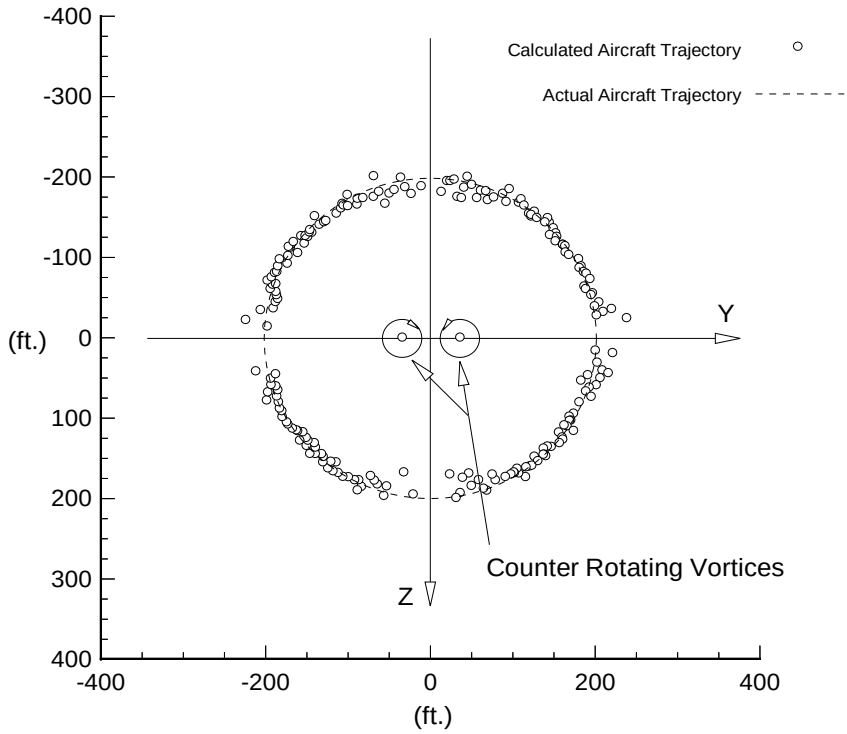

Figure 9. Circular wake vortex encounter and position solutions with $\varepsilon_{total}=0.01^{\circ}$. (P3-PA28)

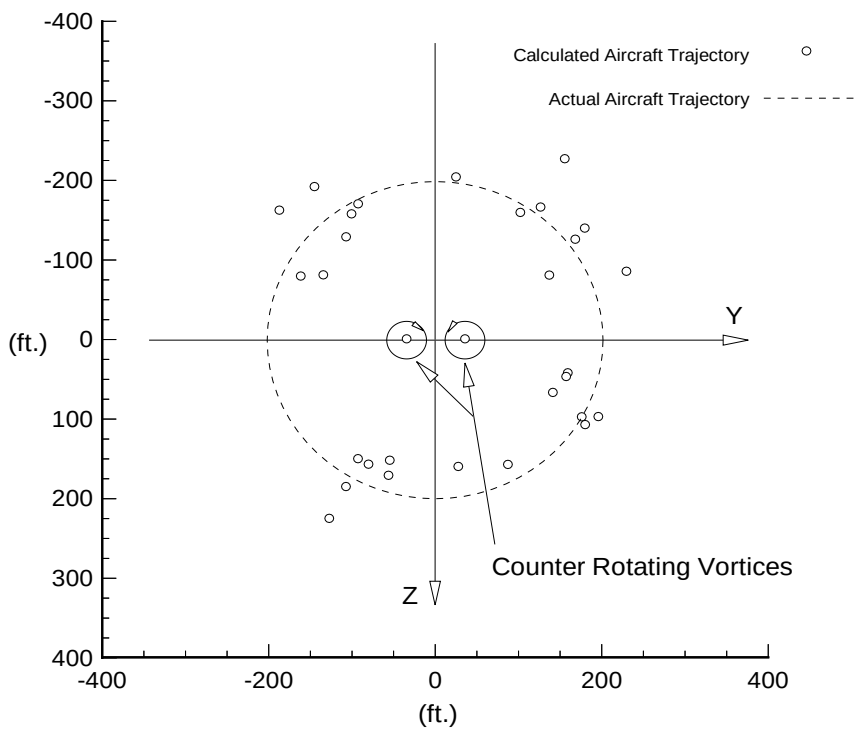

Figure 10. Circular wake vortex encounter and position solutions with $\varepsilon_{total}=0.1^{\circ}$. (P3-PA28)

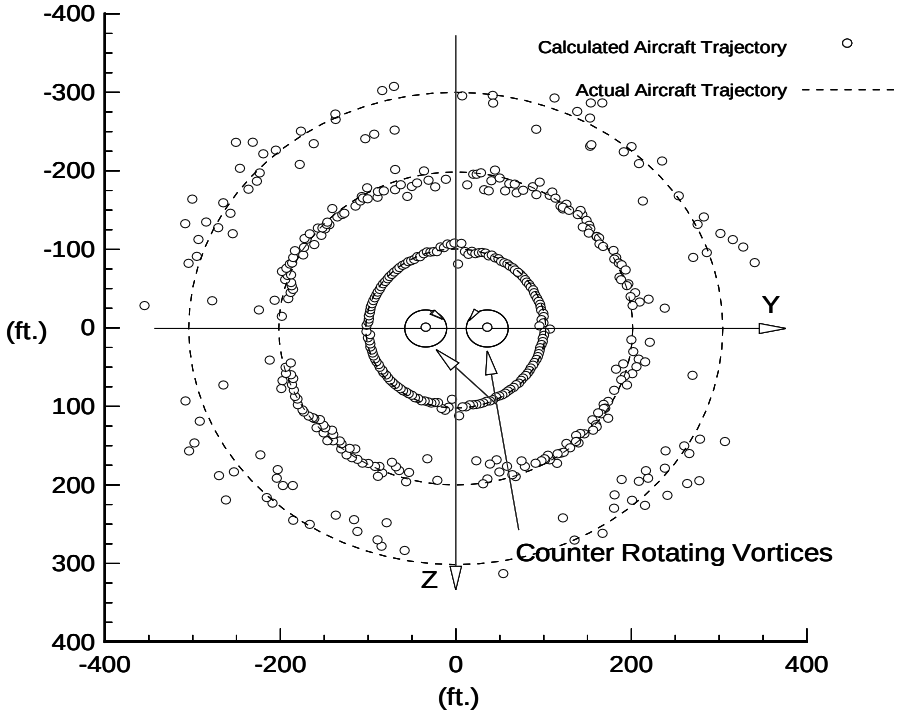

Figure 11. Concentric circular wake vortex encounter tracks and solutions with ε_{total}= 0.01°. (P3-PA28)

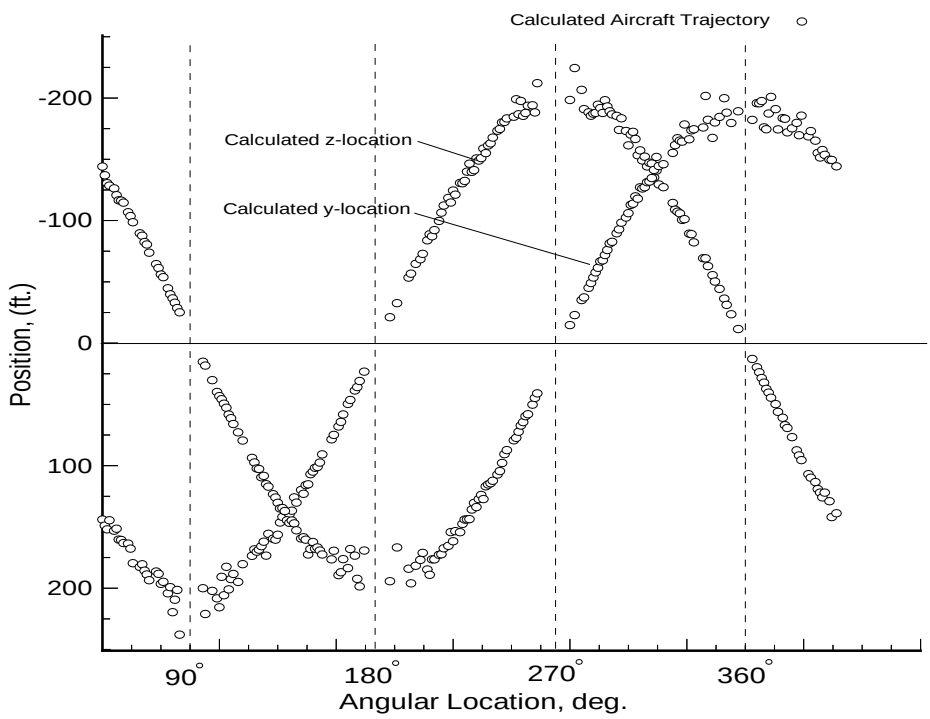

Figure 12. Time history of vertical and horizontal solution locations for circular wake vortex encounter track with ε_{total}= 0.05°. (P3-PA28, Radius = 200 ft.)

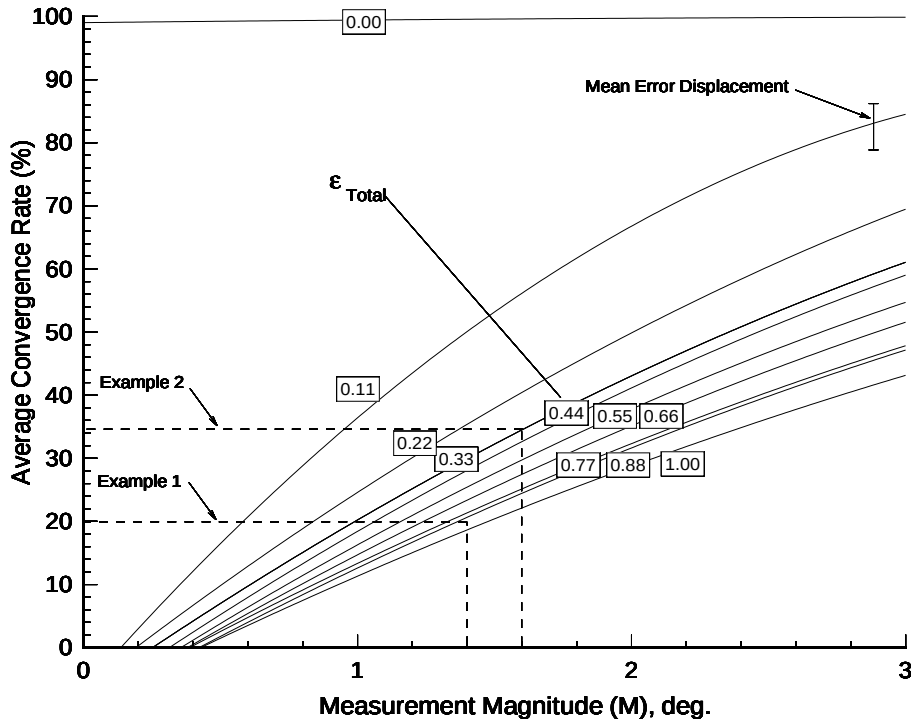

Figure 13. Effect of measurement error (ε_{total}) on convergence rate.

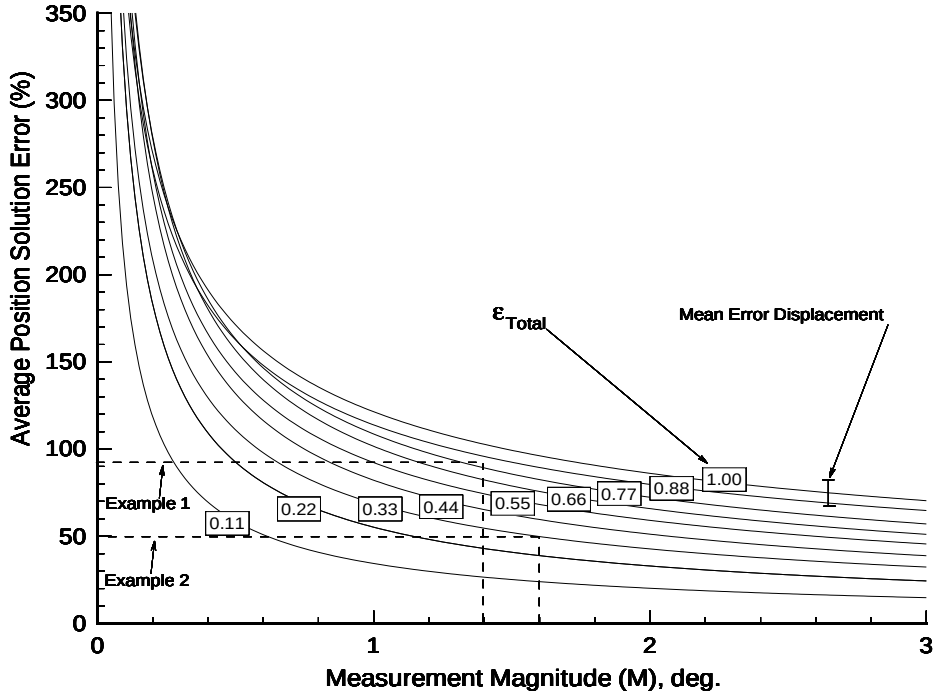

Figure 14. Effect of measurement error (ε_{total}) on position solution error.

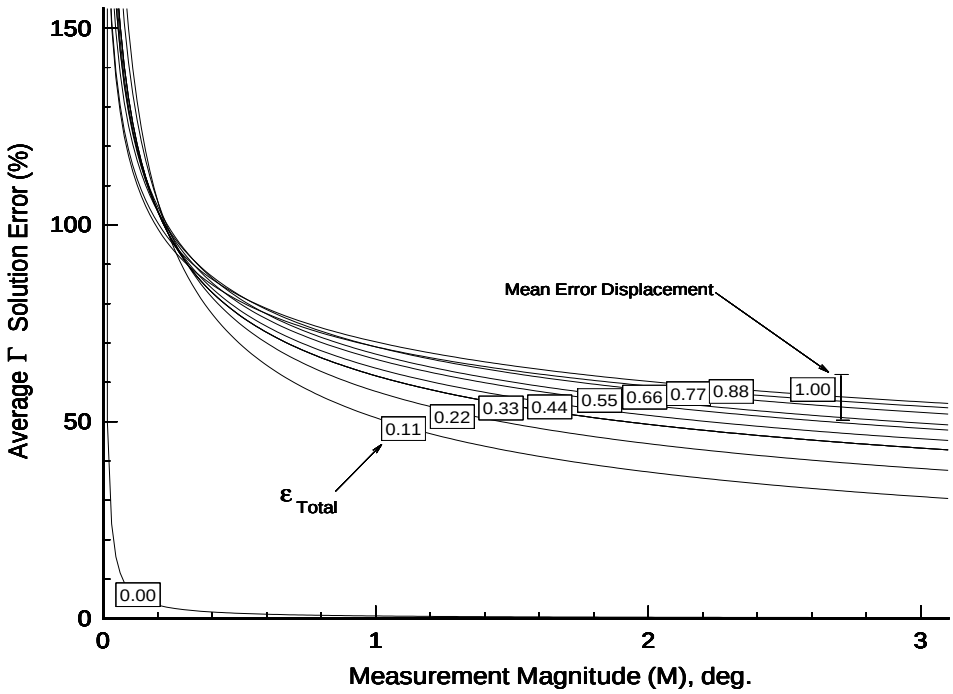

Figure 15. Effect of measurement error (ε_{total}) on average vortex strength (Γ) solution error.

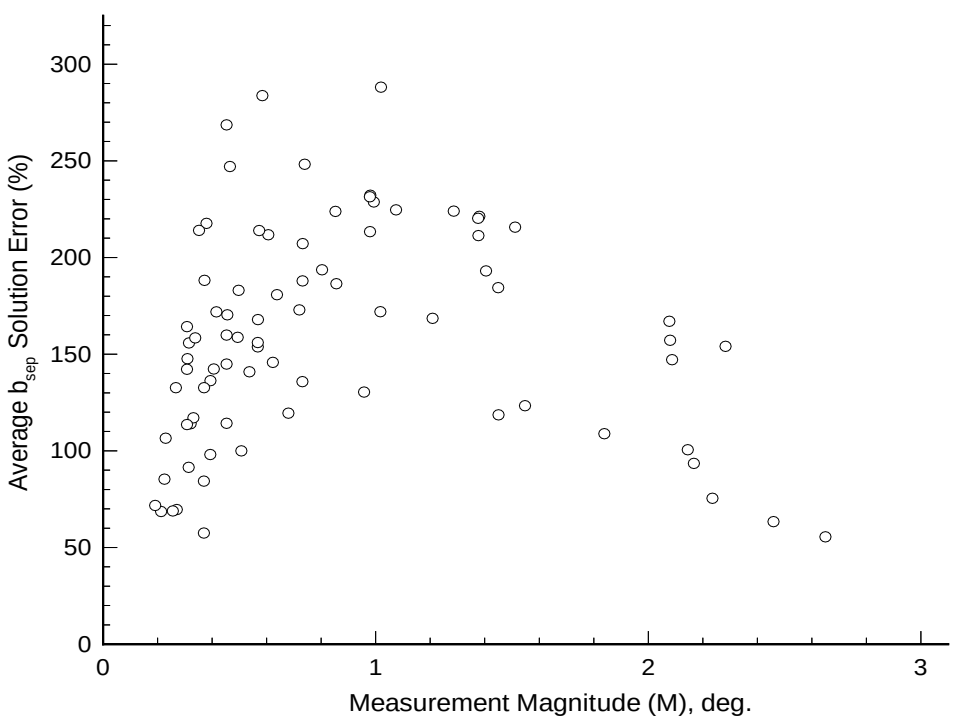

Figure 16. Variance of separation distance (b_{sep}) with measurement magnitude (M). ε_{total}= 0.33°